Case report

Tomoelastography for non-invasive detection of ameloblastoma and metastatic neck lymph nodes

Marie Beier,[1] Ingolf Sack,[2] Benedicta Beck-Broichsitter,[1] Bernd Hamm,[2] Stephan Rodrigo Marticorena Garcia [2]

[1]Department of Oral and Maxillofacial Surgery, Charité – Universitätsmedizin Berlin, corporate member of Freie Universität Berlin, Humboldt-Universität zu Berlin, and Berlin Institute of Health, Berlin, Germany
[2]Department of Radiology, Charité – Universitätsmedizin Berlin, corporate member of Freie Universität Berlin, Humboldt-Universität zu Berlin, and Berlin Institute of Health, Berlin, Germany

Correspondence to
Dr Stephan Rodrigo Marticorena Garcia;
stephan.marticorena-garcia@charite.de

Accepted 12 August 2020

To cite: Beier M, Sack I, Beck-Broichsitter B, *et al*. *BMJ Case Rep* 2020;**13**:e235930. doi:10.1136/bcr-2020-235930

SUMMARY

Ameloblastoma is a benign epithelial tumour and the most common odontogenic tumour, accounting for about 18% of cases. We present a patient to illustrate the first use of tomoelastography for quantitatively mapping tissue stiffness (shear wave speed) and fluidity (loss angle of the complex shear modulus) in a metastasised ameloblastoma of the left mandible. Tomoelastography maps clearly depicted the extent of the tumour by abnormally high values of stiffness and fluidity (1.73±0.23 m/s, 1.18±0.08 rad) compared with normal values in the contralateral mandible (1.04±0.09 m/s, 0.93±0.12 rad). Abnormal stiffness also revealed metastatic involvement of the neck lymph nodes (1.30±0.03 m/s vs 0.86±0.01 m/s). Taken together, stiffness and fluidity measured by tomoelastography can sensitively detect the presence and extent of bone tumours and metastatic spread to cervical lymph nodes.

BACKGROUND

With an annual incidence of 0.5 new cases in 1 000 000 people, ameloblastoma is considered a rare disease.[1] However, in Europe and the USA, ameloblastoma is one of the most common odontogenic tumours after odontoma.[2] Ameloblastoma is a benign epithelial odontogenic tumour that typically develops from proliferating odontogenic epithelium, for example, from enamel residues.[3 4] More than 80% of ameloblastomas are located in the posterior/molar region.[5 6] They are characterised by slow growth but aggressive and locally invasive behaviour.[1 7] Only about 2% of ameloblastomas are malignant with metastatic spread.[1 8–10] The 2017 WHO classification distinguishes three subtypes: unicystic/conventional (previously solid/multicystic), peripheral/extrabony[11] and metastatic.[12] Further subtypes such as follicular and plexiform are distinguished histologically.[13]

Ameloblastomas affect both sexes equally, and their incidence is highest between the second and fourth decade of life with regional differences in prevalence.[14 15] Early ameloblastoma causes no symptoms and is often diagnosed incidentally. Occasional symptoms such as movable teeth, malocclusion or nasal obstruction and pain, and sensory disturbances have been described.[2] Treatment approaches reported in the literature depend on the histological subtype and range from radical to marginal resection or enucleation. Due to the high recurrence rate, which is between 5% and 15% for resection and as high as 55%–90% for less invasive therapies (enucleation and curettage),[6] aggressive resection with safety margins of 0.5–2 cm is recommended.[2 13]

Panoramic radiography, three-dimensional cone-beam CT (3D CBCT) and CT are the primary imaging techniques for the diagnosis of ameloblastoma. In panoramic radiographs or CT scans, ameloblastomas appear as roundish, sharply defined translucent/hypodense lumps, sometimes as multicystic lesions, see 3D CBCT images in figure 1. Because quantitative imaging markers are still lacking, tumour grading and treatment monitoring usually rely on size criteria and morphological changes alone. Recently introduced as a new variant of magnetic resonance elastography (MRE), tomoelastography provides high-resolution quantitative maps of mechanical parameters of soft biological tissues including tumours.[16–18]

In the following, we present the first use of tomoelastography for the diagnosis of a malignant ameloblastoma in a patient. The case illustrates that tomoelastography based on a short MRI scan of 5 min provides useful quantitative information on the local tumour extent and metastatic spread to adjacent lymph nodes.

CASE PRESENTATION

A 53-year-old athletic man with no family history of malignant disease was referred to the Department of Oral and Maxillofacial Surgery of our hospital by a dentist who noticed a progressive swelling and loosened teeth in the area of the left lower jaw. The symptoms started about 1.5 years earlier with undefined and dull pain and recurring swelling in the left mandibular area. The physical examination revealed an asymmetry in the left lower facial region, a firm swelling of the mandibular body and ramus (figure 2), no paraesthesia in the left lower trigeminal nerve distribution (V3) and no palpable cervical lymphadenopathy. There was loosening of molars and premolars of the left mandible. No B-symptoms were present. The patient had no previous illnesses and did not take any medication. He reported no known allergies and no history of smoking and alcohol consumption.

INVESTIGATIONS

A 3D CBCT examination performed 2 years before surgery, which served as baseline, showed a large, hypodense, space-occupying, cystic lesion

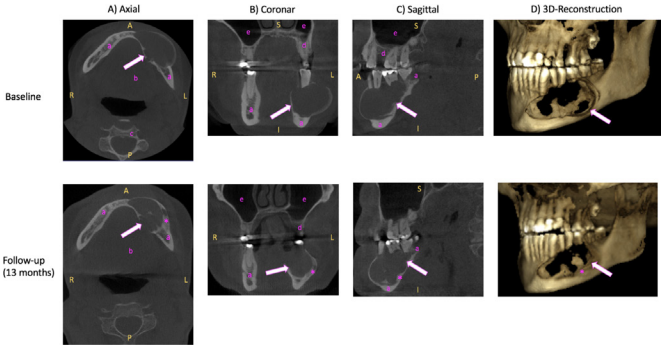

Figure 1 Three-dimensional (3D) cone-beam computed tomography (CBCT) of the mandible. (A) Axial, (B) coronal, (C) sagittal view and (D) 3D reconstruction of unenhanced CBCT images of the ameloblastoma (arrow) in the left mandible at baseline (2 years before surgery, upper line) and at follow-up 1.5 years after the baseline examination (lower line). Baseline (upper row): Ameloblastoma (arrow) appears as roundish, sharply defined hypodense lump. Follow-up (lower line): Compared with baseline, the ameloblastoma (arrow) appears more sclerosed (asterisk) at the edges with relative size constancy. R, right; L, left; A, anterior; P, posterior; S, superior; I, inferior; a, mandible; b, floor of the mouth; c, vertebral body; d, maxilla; e, sinus maxillaris.

respecting the periosteum in the left mandible and measuring 24×48×25 mm (width×depth×height). Brightening of the roof tips was observed in the adjacent molars and premolars in regions 34–36. Odontogenic keratocyst and ameloblastoma were considered as possible diagnoses. Unenhanced axial, coronal, sagittal CT images and 3D reconstructions are provided in the upper row of figure 1.

A biopsy confirmed the diagnosis of an ameloblastoma with metastatic neck lymph nodes. Histopathological images are provided in figure 3. However, the patient refused the surgical removal of the tumour and presented 1.5 years later with progressive complaints due to further tumour growth. A follow-up 3D CBCT examination performed at this time (see lower row in figure 1). Compared with baseline 1.5 years earlier, the mass appears more sclerosed at the edges, as a sign of a chronic reactive response, while its size appears to be relatively constant at 24×45×25 mm. The patient agreed to have surgery, and further diagnostic workup was performed.

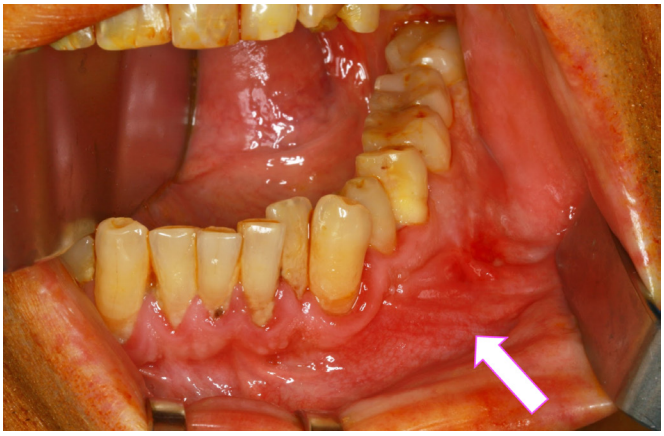

Figure 2 Anterolateral view of the patient's mandible. An arrow indicates the ameloblastoma in the left mandible. In this region, prolapsed tissue and mucosal redness are visible.

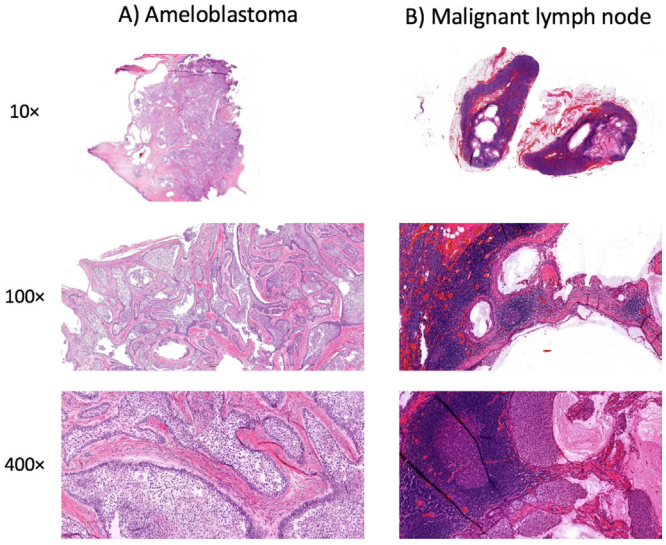

Figure 3 Histopathological sections of the (A) ameloblastoma and (B) malignant lymph nodes. H&E staining with 10-fold, 100-fold and 400-fold magnification.

The patient underwent an MRI examination (1.5 Tesla, Magnetom Sonata, Siemens Erlangen, Germany). The protocol included standard T1-weighted and T2-weighted MRI sequences for anatomical correlation and multifrequency MRE with tomoelastography postprocessing.[16 17] Four mechanical stimulation frequencies of 20, 30, 40 and 50 Hz were induced by two external custom-made pressurised air drivers[17] positioned at the occiput (figure 4). Axially oriented wave images were acquired in 25 slices of 3.0 mm thickness using a single-shot spin-echo echo-planar imaging sequence as described elsewhere.[16] Tomoelastography provides full-field-of-view maps of two parameters: (1) shear wave speed (SWS in m/s) as a surrogate of stiffness and (2) loss angle of the complex shear modulus (ϕ in rad) as a measure of tissue fluidity (ϕ values above the limit of $\pi/4 \approx 0.78$ are considered to indicate a predominance of fluid tissue properties).[18] The total acquisition time of the tomoelastography scan was 5 min with the patient breathing normally.

T1-weighted and T2-weighted MR images demonstrated a hyperintense left mandibular mass with focal thickening but not extending into the periosteum. SWS and ϕ of the mass were higher (1.73±0.23 m/s, 1.18±0.08 rad) compared with reference structures in the contralateral mandible (1.04±0.09 m/s, 0.93±0.12 rad). The abnormally high SWS and ϕ pixel values indicating the extent of the tumour are apparent to the naked eye in figure 5.

Two lymph nodes at level 1b on the left are presented in figure 6. The histopathologically confirmed metastatic lymph node (white, bright arrow; 1.30±0.03 m/s) shows higher SWS than the benign node (magenta, thin arrow; 0.86±0.01 m/s), while fluidity ϕ (malignant vs benign, 0.63±0.03 m/s vs 0.65±0.05 rad) and maximum diameter (6.0 vs 7.0 mm) are not different.

DIFFERENTIAL DIAGNOSIS

It is typically not possible to differentiate ameloblastoma from other osteolytic processes (eg, odontogenic keratocyst) using conventional radiographs and 3D imaging modalities including CT and CBCT.[19] In our patient, the ameloblastoma was initially thought to be a dentogenic cyst so that valuable time passed before the mass was resected.

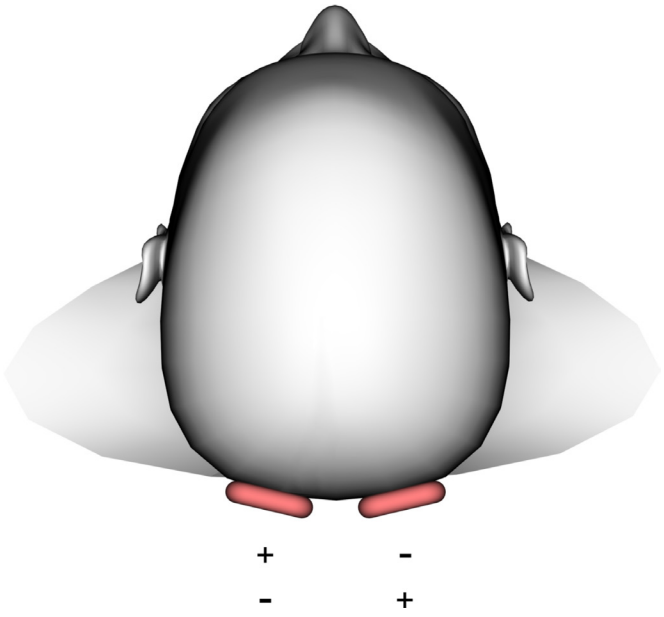

Figure 4 Occipital driver setup. Drivers are highlighted in red. Plus and minus symbols indicate alternating excitation.

TREATMENT

Virtual surgical planning based on CBCT images was used to create individual resection templates and patient-specific miniplates. The operation was performed under general anaesthesia without muscle relaxation, since triggering a muscle contraction by mechanical or electrical stimulation of the marginal branch of the facial nerve and of the hypoglossal and accessory nerves helps to localise and preserve these nerves. The patient was placed in a supine position with the neck stretched and head turned to the opposite side. The neck was opened through a horizontal incision placed in a skin fold just 3–4 cm below the mandibular base. The incision was made through the skin, subcutaneous fat and the platysma muscle, followed by identification of the external jugular vein and the major auricular nerve. After tracheotomy, a segmental resection from the left second molar to the second right incisor and an ipsilateral selective neck dissection of levels 1–3 were performed (figure 7). Fat and lymph nodes were resected from the submental triangle and between the anterior belly of the digastric and mylohyoid muscle. The resulting bone defect was reconstructed with a microvascular anastomosed-free fibula flap containing two segments from the left side and harvested at the same time in a two-team approach. Atherosclerosis and other vessel pathologies were excluded previously by CT angiography. The osteosynthesis was done using computer-aided designed and computer-aided manufactured (CAD/CAM) miniplates (figure 8). The distal and proximal osteotomy was performed with an electric saw after insertion of two protective raspatories and fixation of the resection guides. The vessels within the resection area were ligated. The posterior tibial muscle, the long hallucis flexor muscle and an approximately 10×5 cm portion of the crural fascia as well as the skin of the lower leg corresponding in size to the intraoral mucosal defect were included in the flap design in order to restore the floor of the mouth by secondary healing. After completion of the flap harvest, the CAD/CAM miniplates were fixed between the fibula segments with 2.0 mm monocortical

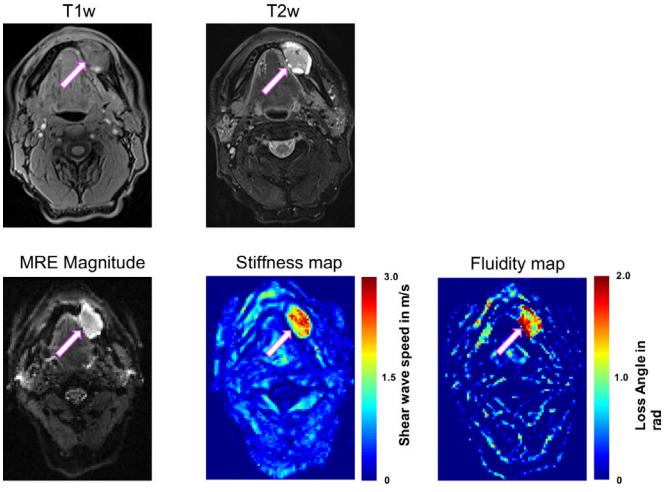

Figure 5 Axial T1-weighted (T1w; VIBE DIXON) and T2-weighted (T2w; TSE DIXON, fat saturated) MR images and magnetic resonance elastography (MRE) magnitude, stiffness and fluidity maps of the ameloblastoma (arrow) in the left mandible. High stiffness and fluidity allow clear identification of the tumour extent. Scale; stiffness, red=stiff, blue=soft; fluidity, red=fluid, blue=solid. Volumetric interpolated breath-hold examination (VIBE)-Dixon, fat saturated; Turbo-Spin-Echo (TSE)-Dixon, fat saturated.

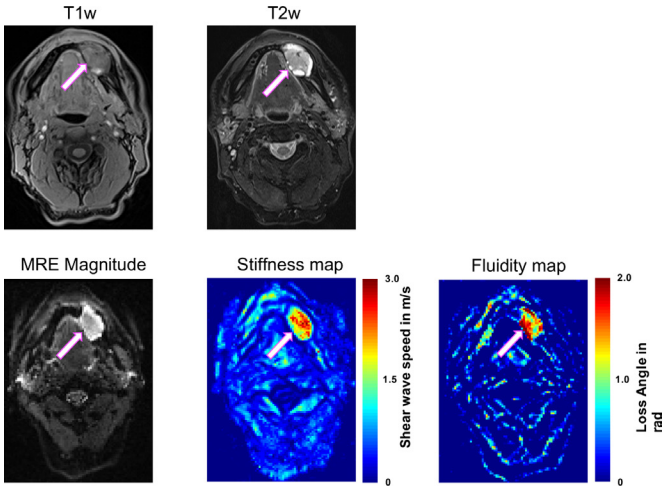

Figure 6 Axial T1-weighted (T1w; VIBE DIXON) and T2-weighted (T2w; TSE DIXON, fat saturated) MR images and magnetic resonance elastography (MRE) magnitude, stiffness map and fluidity map of two small submandibular lymph nodes at level 1b on the left. A histologically confirmed malignant lymph node (bright white arrow) is stiffer than a benign lymph node (thin magenta arrow). Maximum diameter and fluidity did not differ between the two nodes. High stiffness and fluidity allow clear identification of the tumour extent. Scale; stiffness, red=stiff, blue=soft; fluidity, red=fluid, blue=solid.

Figure 7 (A) Lateral view of the ameloblastoma (bright white arrow) of the left mandible. The lateral resection lines are marked with thin black arrows. (B) Resected specimen including the tumour of region 47–32 with a safety margin of 0.5–2.0 cm. (C) Anterolateral view of the patient after tumour resection.

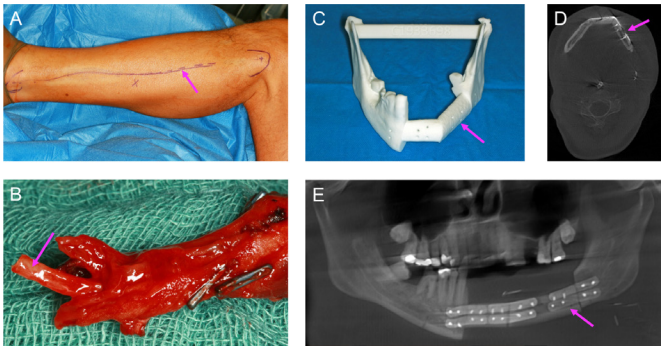

Figure 8 (A) Left lower leg: surgical marks (arrow) for removal of the fibula graft. (B) Microvascular-anastomosed two-segment fibula graft. The vascular stumps (arrows) in the left lower leg were anastomosed with the ipsilateral facial artery and a lateral branch of the internal jugular vein. (C) Individual resection template (arrow) created using virtual surgical planning. Osteosynthesis with computer-aided design and computer-aided manufactured miniplates was performed. Postoperative control (D) CT and (E) panoramic radiography. The fibula graft is indicated by an arrow.

screws. The vascular pedicle of the left fibula was anastomosed to the facial artery and a branch of the internal jugular vein, and osteosynthesis with the residual lower jaw was completed with 2.0 mm bicortical screws. The neck was irrigated with water, and a suction drain was inserted and closed in layers to platysma and skin. Finally, successful graft perfusion was confirmed by clinical palpation and observation of graft colour and by Doppler ultrasound.

The histopathological examination showed a solid ameloblastoma arising from the mandible and restricted to the periosteum (figure 7B). The margins were clear and no malignant cells were found at the surgical resection margin. Examination of the cervical lymph nodes removed at level 1b on the left revealed metastatic involvement by ameloblastic tumour in two nodes and no metastatic involvement of four nodes.

OUTCOME AND FOLLOW-UP

The patient's postoperative recovery was uneventful. The patient was observed on an intermediate care unit for one night. The tracheotomy tube was removed after 2 days. He was discharged from hospital after 8 days. Photographs at 2 month postoperative follow-up are provided in figure 9.

The patient is enrolled in a tumour aftercare programme including imaging examinations at regular intervals.

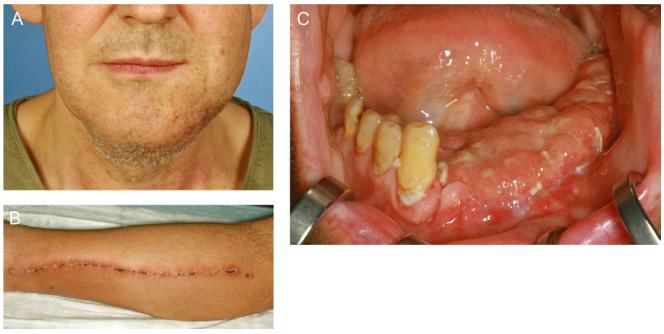

Figure 9 At 2-month follow-up, primary wound healing with scar formation is apparent in the face (A) and left lower leg (B). Granulation tissue in the surgical scar indicates successful graft transplantation (C).

DISCUSSION

This case demonstrates the clinical value of MRI-based tomoelastography for the diagnostic characterisation of a malignant metastatic ameloblastoma.

Metastatic ameloblastoma is rare and no systematic studies are available. Only case reports exist in the literature.[20–22] To the best of our knowledge, this is the first report of the clinical use of MRE or tomoelastography for bone tumour assessment and detection of metastatic lymph nodes in the head and neck. Tomoelastography provided valuable details of the mechanical properties of small anatomical mandibular structures. This case shows that shear waves of sufficient amplitudes for MRE can be generated in the skull bone and mandibular joint.

Interestingly, tomoelastography detects stiffening in malignant lymph nodes, which is in agreement with surgical palpation. This finding is histopathologically confirmed by tumour cell infiltration, accumulation of extracellular matrix components and small numbers of macrophages.[23] Since tomoelastography has not been applied to the neck so far, we discuss our results in comparison with findings obtained in liver tumours using a similar tomoelastography setup. Our results in this patient are consistent with findings in malignant liver tumours, where both stiffness and fluidity were reported to be abnormally high.[18] Of note, tomoelastography-measured fluidity does not depend on the tissue's water content.[24] Instead, it measures the stickiness or motility of particles in a material, which determines internal friction and deformability. The higher fluidity of the tumour we observed in this case indicates a higher degree of mechanical friction. Conventional imaging techniques such as T1-weighted or T2-weighted MRI as well as CT suffer from insufficient sensitivity to malignant lymph nodes. For this reason, the lymph node diameter is typically the only quantitative hint of possible malignancy. CT and MRI are widely used with a high diagnostic accuracy for detection of neck lymph node metastasis above 10 mm (area under the curve, CT=0.84; MRI=0.91).[25] Differences in the T1 and T2 relaxation times do not improve the detection of malignant lymph nodes.[26] The lack of detection of small malignant lymph node metastases (<10 mm) based on T1-weighted and T2-weighted MRI in our patient is consistent with the published data.[27] Positron emission tomography (PET)-CT and PET-MR are considered as reference methods for the detection of metastatic lymph nodes; however, these hybrid modalities are very expensive and not widely available, and they are limited by low spatial resolution and the fact that inflammatory processes can lead to false-positive results.[28] Diffusion-weighted imaging (DWI) is a promising imaging technique for the detection of malignant lymph nodes based on pathologically altered free diffusion of water at the cellular level. In the literature, it has been reported that apparent diffusion coefficients correlate negatively with tumour grade.[29] A recent meta-analysis found a pooled sensitivity and specificity of 90% and 88% for the detection of malignant lymph nodes.[30] However, in another study, adding DWI did not improve the diagnostic accuracy of PET-CT.[31]

In the future, a presurgical non-invasive mechanical characterisation of residual bone marrow by tomoelastography could also be used to predict bone allograft reconstruction stability, and thus help in selecting the most promising material and fixing technique.

Conventional MRE, performed at a single mechanical frequency, often cannot resolve mechanical details on the scale of single pixels. Ultrasound-based elastography methods such as acoustic radiation force impulse techniques are widely available

and used for diagnostic imaging of neck soft tissues, demonstrating stiffening in malignant superficial lymph nodes.[32–34] However, ultrasound-based elastography of bone tumours has not yet been reported—probably due to the limited penetration of transient shear waves and ultrasound impulses into bone.

Tomoelastography offers a unique imaging test for the mechanics-based staging of bone tumours such as ameloblastoma and metastatic lymph nodes by depicting abnormally high values of tissue stiffness and fluidity without the need for radiation exposure or contrast medium administration.

Patient's perspective

Episodes of swelling in the left lower jaw began about 30 years ago. At times, the intervals between two episodes were very long, so that no further examinations were done. Seven or eight years ago, my dentist made an X-ray and diagnosed a cyst. Since I had no symptoms, no further measures were taken. It was only about 1.5 years ago that I began to develop increasing pain and also a persistent swelling in the region. My dentist then took a sample. I was informed that it was a benign tumour that could be operated on and removed in hospital. I then presented to the special consultation service of the clinic for oral and maxillofacial surgery. The doctor explained the diagnosis to me and informed me in detail about the treatment options, including possible side effects. I decided to have the operation and was given an appointment for inpatient admission. I had never had an operation before and I had reservations about such a major procedure.

Tomoelastography was performed before the operation. The external vibration necessary to generate the waves was quite intense but well tolerable and adapted to my subjective sensation. The radiologist showed me the elastograms. My anatomical orientation was very poor, but I was able to follow the radiologist's explanations, and the tumour area was clearly visible to me without deeper knowledge.

After the operation, I spent one night in the intensive care unit for monitoring. The tracheotomy, which was necessary during the operation, was the worst for me. I could not speak and had a strong irritation of the throat. When this was removed on the second day after the operation, I was really relieved. I had no pain. All in all, I recovered surprisingly quickly from this major operation.

Learning points

- First in vivo detection of bone tumour boundaries based on mechanical properties.
- Ameloblastoma is characterised by abnormally high stiffness and fluidity parameters.
- Tomoelastography sensitively identifies lymph node metastasis by abnormally high stiffness and is a promising non-invasive and quantitative marker for tumour staging.
- Metastatic ameloblastoma should be diagnosed and operated on at an early stage.
- Quantitative cut-off values of stiffness and fluidity are needed for therapeutic decision-making and could be generated for different histological subtypes of ameloblastoma in the future.

Acknowledgements The authors would like to acknowledge PD Dr Jürgen Braun and Felix Schrank for method development and technical support, Professor Dr Dr Max Heiland for clinical support, Dr Iris Piwonski for the preparation and analysis of histopathological images and the patient for his continued engagement and support.

Contributors MB, IS and SRMG: Conception, design, acquisition, analysis and interpretation of the data. Drafting the article. Final approval of the published version. Agreement to be accountable for the article and to ensure data accuracy and integrity. BB and BH: Conception and design. Revising the article critically for important intellectual content. Final approval of the published version. Agreement to be accountable for the article and to ensure data accuracy and integrity.

Funding The authors have not declared a specific grant for this research from any funding agency in the public, commercial or not-for-profit sectors.

Competing interests None declared.

Patient consent for publication Obtained.

Provenance and peer review Not commissioned; externally peer reviewed.

ORCID iD
Stephan Rodrigo Marticorena Garcia http://orcid.org/0000-0003-3782-3003

REFERENCES

1 Kreppel M, Zöller J. Ameloblastoma-Clinical, radiological, and therapeutic findings. *Oral Dis* 2018;24:63–6.
2 Giraddi GB, Arora K, Saifi AM. Ameloblastoma: a retrospective analysis of 31 cases. *J Oral Biol Craniofac Res* 2017;7:206–11.
3 Hong J, Yun P-Y, Chung I-H, *et al*. Long-Term follow up on recurrence of 305 ameloblastoma cases. *Int J Oral Maxillofac Surg* 2007;36:283–8.
4 Schwenzer NEM. *Zahnärztliche Chirurgie*, 2019.
5 Hansen T, Bogumil A, Koutsimpelas D. [Primary plexiform ameloblastoma in the sinonasal tract of a 49-year-old female patient. Case report]. *HNO* 2013;61:673–6.
6 Celur S, Babu KS. Plexiform ameloblastoma. *Int J Clin Pediatr Dent* 2012;5:78–83.
7 Ruslin M, Hendra F-N, Vojdani A, *et al*. The epidemiology, treatment, and complication of ameloblastoma in East-Indonesia: 6 years retrospective study. *Med Oral Patol Oral Cir Bucal* 2018;23:e54–8.
8 Balasubramaniam S, Jayaraman B, Thirunavukkarasu R, *et al*. Recurrent ameloblastoma 24 years after hemimandibulectomy: a case report and review of literature. *Indian J Dent Res* 2019;30:960–3.
9 Haq J, Siddiqui S, McGurk M. Argument for the conservative management of mandibular ameloblastomas. *Br J Oral Maxillofac Surg* 2016;54:1001–5.
10 Malphrus EL, Mantilla-Rivas E, Bryant JR, *et al*. Hemimandibular reconstruction of pediatric ameloblastoma with templated free fibula flap. *Plast Reconstr Surg Glob Open* 2019;7:1.
11 Seki-Soda M, Sano T, Ito K, *et al*. An immunohistochemical and genetic study of $BRAF^{V600E}$ mutation in Japanese patients with ameloblastoma. *Pathol Int* 2020;70:224–30.
12 Kitisubkanchana J, Reduwan NH, Poomsawat S, *et al*. Odontogenic keratocyst and ameloblastoma: radiographic evaluation. *Oral Radiol* 2020. doi:10.1007/s11282-020-00425-2
13 Dandriyal R, Gupta A, Pant S, *et al*. Surgical management of ameloblastoma: conservative or radical approach. *Natl J Maxillofac Surg* 2011;2:22–7.
14 Patsa S, Jadav RB, Halder GC, *et al*. Demographic and histopathological variation of ameloblastoma: a hospital-based study. *J Oral Maxillofac Pathol* 2016;20:230–3.
15 Dhanuthai K, Chantarangsu S, Rojanawatsirivej S, *et al*. Ameloblastoma: a multicentric study. *Oral Surg Oral Med Oral Pathol Oral Radiol* 2012;113:782–8.
16 Tzschätzsch H, Guo J, Dittmann F, *et al*. Tomoelastography by multifrequency wave number recovery from time-harmonic propagating shear waves. *Med Image Anal* 2016;30:1–10.
17 Marticorena Garcia SR, Hamm B, Sack I. Tomoelastography for non-invasive detection and treatment monitoring in acute appendicitis. *BMJ Case Rep* 2019;12. doi:10.1136/bcr-2019-230791. [Epub ahead of print: 26 Aug 2019].
18 Shahryari M, Tzschätzsch H, Guo J, *et al*. Tomoelastography distinguishes noninvasively between benign and malignant liver lesions. *Cancer Res* 2019;79:5704–10.
19 Sheela S, Singer SR, Braidy HF, *et al*. Maxillary ameloblastoma in an 8-year-old child: a case report with a review of the literature. *Imaging Sci Dent* 2019;49:241–9.
20 Broudic-Guibert M, Blay J-Y, Vazquez L, *et al*. Persistent response to vemurafenib in metastatic ameloblastoma with BRAF mutation: a case report. *J Med Case Rep* 2019;13:245.
21 Brunet M, Khalifa E, Italiano A. Enabling precision medicine for rare head and neck tumors: the example of BRAF/MEK targeting in patients with metastatic ameloblastoma. *Front Oncol* 2019;9:1204.
22 Li D, Xu S, Sun M, *et al*. Maid chemotherapy regimen as a treatment strategy for metastatic malignant ameloblastoma: a case report. *Medicine* 2019;98:e15873.
23 Alderton GK. Metastasis: active lymph nodes. *Nat Rev Cancer* 2013;13:606–7.
24 Streitberger K-J, Lilaj L, Schrank F, *et al*. How tissue fluidity influences brain tumor progression. *Proc Natl Acad Sci U S A* 2020;117:128–34.

25 Sun J, Li B, Li CJ, *et al*. Computed tomography versus magnetic resonance imaging for diagnosing cervical lymph node metastasis of head and neck cancer: a systematic review and meta-analysis. *Onco Targets Ther* 2015;8:1291–313.
26 Vandecaveye V, De Keyzer F, Vander Poorten V, *et al*. Head and neck squamous cell carcinoma: value of diffusion-weighted MR imaging for nodal staging. *Radiology* 2009;251:134–46.
27 Jin GQ, Yang J, Liu LD, *et al*. The diagnostic value of 1.5-T diffusion-weighted MR imaging in detecting 5 to 10mm metastatic cervical lymph nodes of nasopharyngeal carcinoma. *Medicine* 2016;95:e4286.
28 Vandecaveye V, De Keyzer F, Hermans R. Diffusion-Weighted magnetic resonance imaging in neck lymph adenopathy. *Cancer Imaging* 2008;8:173–80.
29 Jović A, Fila J, Gršić K, *et al*. Diffusion-Weighted MRI: impact of the size of the Roi in detecting metastases in subcentimeter lymph nodes in head and neck squamous cell carcinoma. *Neuroradiology* 2020;62:987–94.
30 Suh CH, Choi YJ, Baek JH, *et al*. The diagnostic value of diffusion-weighted imaging in differentiating metastatic lymph nodes of head and neck squamous cell carcinoma: a systematic review and meta-analysis. *AJNR Am J Neuroradiol* 2018;39:1889–95.
31 Noij DP, Martens RM, Zwezerijnen B, *et al*. Diagnostic value of diffusion-weighted imaging and ^{18}F-FDG-PET/CT for the detection of unknown primary head and neck cancer in patients presenting with cervical metastasis. *Eur J Radiol* 2018;107:20–5.
32 Tan S, Miao L-Y, Cui L-G, *et al*. Value of shear wave elastography versus contrast-enhanced sonography for differentiating benign and malignant superficial lymphadenopathy unexplained by conventional sonography. *J Ultrasound Med* 2017;36:189–99.
33 Chae SY, Jung HN, Ryoo I, *et al*. Differentiating cervical metastatic lymphadenopathy and lymphoma by shear wave elastography. *Sci Rep* 2019;9:12396.
34 Chen B-B, Li J, Guan Y, *et al*. The value of shear wave elastography in predicting for undiagnosed small cervical lymph node metastasis in nasopharyngeal carcinoma: a preliminary study. *Eur J Radiol* 2018;103:19–24.